

# A Coordinate Descent Approach to Atomic Norm Minimization

Ruifu Li , Danijela Cabric, *Fellow, IEEE*

**Abstract**—Atomic norm minimization is of great interest in various applications of sparse signal processing including super-resolution line-spectral estimation and signal denoising. In practice, atomic norm minimization (ANM) is formulated as a semi-definite programming (SDP) which is generally hard to solve. This work introduces a low-complexity, matrix-free method for solving ANM. The method uses the framework of coordinate descent and exploits the sparsity-induced nature of atomic-norm regularization. Specifically, an equivalent, non-convex formulation of ANM is first proposed. It is then proved that applying the coordinate descent framework on the non-convex formulation leads to convergence to the global optimal point. For the case of a single measurement vector of length  $N$  in discrete fourier transform (DFT) basis, the complexity of each iteration in the coordinate descent procedure is  $\mathcal{O}(N \log N)$ , rendering the proposed method efficient even for large-scale problems. The proposed coordinate descent framework can be readily modified to solve a variety of ANM problems, including multi-dimensional ANM with multiple measurement vectors. It is easy to implement and can essentially be applied to any atomic sets as long as a corresponding rank-1 problem can be solved. Through extensive numerical simulations, it is verified that for solving sparse problems the proposed method is much faster than the alternating direction method of multipliers (ADMM) or the customized interior point SDP solver.

**Index Terms**—Super resolution, Coordinate Descent, Atomic Norm, Denoising, Low Complexity

## I. INTRODUCTION

IN the post compressed sensing era, ANM is a powerful candidate for finding a sparse representation of a measured signal as it resolves the basis mismatch problem [1] that typically arises for DFT basis. The advantage of atomic norm originates from its definition: it is defined based on a continuous manifold referred to as the atomic set. As opposed to a basis of a finite number of vectors which typically arises in  $\ell_1$ -norm regularized least-square regression, the atomic set contains infinitely many vectors. Consequently, the reconstruction from an atomic norm regularized least-square regression tends to be more sparse than its counterpart regularized by  $\ell_1$  norm, as the representation can consist of any points on a continuous manifold. This feature makes ANM a powerful tool in estimations of continuous parameters (delay, frequencies, Doppler, etc) where super resolution is required, as well as denoising applications of discrete signals such as images or speeches.

The price to pay for searching over a continuous dictionary is the amount of computations required to obtain the solution.

Ruifu Li and Danijela Cabric are with the Electrical and Computer Engineering Department, University of California, Los Angeles, Los Angeles, CA 90095 (e-mail: doanr37@ucla.edu; danijela@ee.ucla.edu).

This work is supported by NSF under grant 1718742 and 1955672.

Unlike constrained least-square problems, ANM is originally formulated as an SDP in the seminal paper [2]. The SDP is based on the bounded real lemma [3] which characterizes the infinite-dimensional constraint. From then, the SDP formulation of ANM has been applied extensively to various estimations of grid-less parameters. For a  $N$ -dimensional complex vector  $\mathbf{y} \in \mathbb{C}^N$ , the cost of solving ANM is  $\mathcal{O}(N^4)$  if a general purpose interior-point solver is used [4], and  $\mathcal{O}(N^3)$  with the customized interior-point solver [5] or with the proximal methods [6]. For the ANM problem of multiple measurement vector (MMV)  $\mathbf{y}_1, \mathbf{y}_2, \dots, \mathbf{y}_M$ , the cost increases to  $\mathcal{O}(N+M)^3$  [7] per iteration. Such expensive computational complexity poses serious limitations on the applicability of ANM for large-scale problems where  $N$  or  $M$  is on the order of  $10^4$  or higher. In spite of this, ANM is still considered to be one of most popular tool in many applications of super-resolution. Over the years, numerous variants of ANM are developed including ANM with decoupled formulations [8], with multi-dimensional frequency estimation [9] and with weighted atomic set [10]. It is also applied to signal denoising [11], linear system identification [12], and wireless channel estimation [13], etc.

To fill the gap on efficient solvers of ANM, this work provides an iterative, low-complexity framework. The method is based on coordinate descent algorithm and is easy to implement. The method originates from a mixed-integer but equivalent formulation of the ANM. Namely, it shares the same global optimal point as that of the SDP formulation. More importantly, the mixed-integer formulation automatically integrates the semi-definite constraint after which the coordinate descent method is readily applicable. The main advantages of the proposed framework include:

- For the classic basis of DFT vectors, the method is essentially matrix-free. With fast fourier transform (FFT), the cost per-iteration is  $\mathcal{O}(N \log N)$ .
- The method can be readily customized to solve a variety of ANM problems, including mutli-dimensional, multi-snapshot, as well as weighted ANM problems. Theoretically, the method can also work with any atomic sets.
- The method has high flexibility and admits customized initialization. For instance, one can first solve the on-grid least absolute shrinkage and selection operator (LASSO) regression as a warm start and then apply the method to resolve the off-grid errors.
- The method has rapid convergence when the optimal solution has a sparse structure.

Applying the coordinate descent method to sparse recovery

problem has been previously studied for the LASSO regression [14], [15]. It is demonstrated that the method can converge to the global optimal. Similarly, this work provides a simple proof that the coordinate descent procedure would asymptotically converge to the solution of the SDP formulation of ANM. The rest of the paper is organized as follows. In II, we briefly introduce preliminary background and related work. The proposed coordinate descent framework is discussed in III. The extension of the method to various ANM problems are presented in IV. Section V presents simulation results as well as comparison with other state of the art (SOTA) methods. Discussion and future work suggestions are in Section VI. The paper is concluded in Section VII.

*Notations:* Scalars, vectors, and matrices are denoted by non-bold, bold lower-case, and bold upper-case letters, respectively, e.g.  $h$ ,  $\mathbf{h}$  and  $\mathbf{H}$ . The element in  $i$ -th row and  $j$ -th column in matrix  $\mathbf{H}$  is denoted by  $[\mathbf{H}]_{i,j}$ . Transpose and Hermitian transpose are denoted by  $(\cdot)^T$  and  $(\cdot)^H$ , respectively. The  $l_p$ -norm of a vector  $\mathbf{h}$  is denoted by  $\|\mathbf{h}\|_p$ .  $\text{diag}(\mathbf{A})$  aligns diagonal elements of  $\mathbf{A}$  into a vector, and  $\text{diag}(\mathbf{a})$  aligns vector  $\mathbf{a}$  into a diagonal matrix. The operator  $\mathcal{T}(\cdot)$  denotes the mapping from a vector to a Toeplitz matrix with first column being the vector provided. The inner product between two elements  $\mathbf{x}, \mathbf{y}$  from a vector space  $\mathbf{x}, \mathbf{y}$  is denoted as  $\langle \mathbf{x}, \mathbf{y} \rangle$ . Unless otherwise stated, it is assumed that the  $l_2$ -norm can be induced by the inner product, i.e.,  $\|\mathbf{x}\|_2^2 = \langle \mathbf{x}, \mathbf{x} \rangle$ . For a countable set  $\mathcal{S}$ ,  $|\mathcal{S}|$  denote the number of elements in  $\mathcal{S}$ , while  $[\mathcal{S}]_i$  denote the  $i$ -th element from the set.

## II. PRELIMINARIES AND RELATED WORK

In this section the basic concepts of atomic set and atomic norm are introduced, followed by a brief overview on the applications of ANM and related studies.

In short, the atomic norm generalizes the notion of  $l_1$ -norm to a continuous basis. In a  $N$ -dimensional vector space, consider the classical problem of representing a signal  $\mathbf{y}$  with elements  $\mathbf{a}_i$  from a set of basis  $\mathcal{A}$ . In the celebrated LASSO regression, the basis set  $\mathcal{A}$  is usually finite and over complete which can be represented as a matrix  $\mathbf{A} = [\mathbf{a}_0, \mathbf{a}_1, \dots, \mathbf{a}_i, \dots]$ . A sparse representation can be induced simply by adding  $l_1$ -norm regularization to a least square regression, leading to the following optimization problem:

$$\underset{\mathbf{c}}{\text{Minimize}} \quad \|\mathbf{c}\|_1 + \frac{\zeta}{2} \|\mathbf{y} - \mathbf{A}\mathbf{c}\|_2^2 \quad (1)$$

where  $\zeta > 0$  is a positive constant that balances the error and the sparsity of the solution. When the basis set  $\mathcal{A}$  contains infinitely many elements, an matrix presentation like (1) is no longer available. Instead of  $l_1$ -norm, the regularization is now based on the atomic norm  $\|\cdot\|_{\mathcal{A}}$ . The correspondence to (1) with an infinite-dimensional set of basis  $\mathcal{A}$  is the atomic norm soft thresholding (AST) [11]:

$$\underset{\mathbf{x}}{\text{Minimize}} \quad \|\mathbf{x}\|_{\mathcal{A}} + \frac{\zeta}{2} \|\mathbf{y} - \mathbf{x}\|_2^2 \quad (2)$$

with  $\|\mathbf{x}\|_{\mathcal{A}}$  defined as:

$$\|\mathbf{x}\|_{\mathcal{A}} = \inf \{t > 0 \mid \mathbf{x} \in t \cdot \text{conv}(\mathcal{A})\} \quad (3)$$

The definition (3) is abstract<sup>1</sup> as it involves the concept of a convex hull  $\text{conv}(\mathcal{A})$  of the infinite-dimensional set  $\mathcal{A}$ . Fortunately, as long as the set  $\mathcal{A}$  is symmetrical with respect to the origin, the definition (3) can be equivalently interpreted from a total variation perspective [3]:

$$\|\mathbf{x}\|_{\mathcal{A}} = \inf \left\{ \sum_i c_i \mid \mathbf{x} = \sum_i c_i \mathbf{a}_i, c_i > 0, \mathbf{a}_i \in \mathcal{A} \right\} \quad (4)$$

With the definition (4), a mixed-integer formulation of ANM can be derived accordingly:

$$\underset{L, c_i \geq 0, \mathbf{a}_i \in \mathcal{A}}{\text{Minimize}} \quad \sum_i c_i + \frac{\zeta}{2} \left\| \mathbf{y} - \sum_i c_i \mathbf{a}_i \right\|_2^2 \quad (5)$$

In section III, the two problems are proved to be equivalent as they shared the same solution. The notion of ANM can be better motivated with its applications. Some most frequently used atomic sets include:

- The set of complex exponential vectors. The set consists of continuous DFT basis defined with a frequency  $f$  over  $[0, 2\pi)$ :

$$\left\{ e^{1j\phi} \mathbf{a}(f) \mid \phi, f \in [0, 2\pi), [\mathbf{a}(f)]_i = e^{1j(i-1)f} \right\} \quad (6)$$

The set naturally arises in a variety of array signal processing and wireless communication problems.

- DFT basis with multiple snapshots. The set consists of continuous DFT basis combined with a unit-norm sphere via the outer-product:

$$\left\{ \mathbf{a}(f) \otimes \mathbf{c} \mid [\mathbf{a}(f)]_i = e^{1j(i-1)f}, \|\mathbf{c}\|_2 = 1 \right\} \quad (7)$$

The set plays a major role in estimation problems with MMV where the observation  $\mathbf{y}$  in (2) becomes a vector  $\mathbf{Y}$  instead of a matrix.

- Two-dimensional DFT basis. The set consists of 2D continuous DFT basis that naturally arises in signal processing problems with a planar array

$$\left\{ e^{1j\phi} \mathbf{a}(f_1) \otimes \mathbf{a}(f_2) \mid [\mathbf{a}(f)]_i = e^{1j(i-1)f} \right\} \quad (8)$$

Plugging either of these atomic sets (6) - (8) into the ANM (2) produces a well-defined convex optimization problem with semi-definite constraints. For instance, with  $\mathcal{A}$  defined as (6), (2) is equivalent to the following SDP [16]:

$$\begin{aligned} & \underset{\mathbf{x}, \mathbf{u}, t}{\text{Minimize}} \quad \frac{t}{2} + \frac{1}{2N} \text{tr}(\mathcal{T}(\mathbf{u})) + \frac{\zeta}{2} \|\mathbf{y} - \mathbf{x}\|_2^2 \\ & \text{subject to} \quad \begin{bmatrix} \mathcal{T}(\mathbf{u}) & \mathbf{x} \\ \mathbf{x}^H & t \end{bmatrix} \succeq 0 \end{aligned} \quad (9)$$

The conversion between (2) to (9) is non-trivial as it relies on the fact that the outer product of a DFT vector with itself produces a hermitian Toeplitz matrix, i.e.,  $\mathcal{T}(\mathbf{a}(f)) = \mathbf{a}(f)\mathbf{a}^H(f)$ . Therefore the SDP formulation (9) cannot be generalized to arbitrary atomic sets. Nevertheless, the legitimate SDP (9) can be solved in polynomial time with several existing algorithms. [3] proposed the well-known ADMM method

<sup>1</sup> [3] delivers an excellent and friendly exposition to ANM that includes more detailed and rigorous discussions on the concept of atomic norm.

to tackle the semi-definite constraints. In each iteration, the complexity of the projection step which requires a singular-value decomposition (SVD) is  $\mathcal{O}(N^3)$ . On the other hand, [5] addressed in detail of a customized primal-dual interior point solver for (9). The computation of the exact Hessian matrix inevitably requires  $\mathcal{O}(N^3)$  computational complexity. [6] proposes the proximal gradient method for a variant of (9) with hard thresholding. The method it proposes has  $\mathcal{O}(N^2)$  complexity per iteration. Different from the works above, rather than focusing on the SDP (9) this work addresses the mixed-integer formulation (5) directly. From such a perspective, the most related method from previous literature is the well-known Newtonized orthogonal matching pursuit (NOMP) [17]. The major limitation of NOMP is that instead of the ANM, it attempts to work with atomic  $\ell_0$  norm  $\|\cdot\|_{\mathcal{A},0}$  regularization. Consequently, due to the highly non-convex nature of the  $\ell_0$  norm, NOMP is not guaranteed to converge to the global optimal point. The discussion in [17] is also limited to the continuous DFT basis (6), (7) and doesn't extend to general atomic sets.

Applying coordinate descent to LASSO problems is discussed by [14], [15]. Although most discussions are limited to the case of a fixed basis (1), they provide inspiration to the algorithmic development in section III-B. In the next section, the equivalence between different ANM formulations are demonstrated, upon which the proposed method is discussed in detail.

### III. THE COORDINATE DESCENT APPROACH FOR GENERAL ANM

The development of the proposed coordinate descent approach starts with the critical observation that the two formulations of ANM (2), (5) share the same solution. To prove this fact, the basic step is to show that the solution of (5) also satisfies the condition of the optimal point for (2). It naturally follows that optimizing each pair  $(c_i, \mathbf{a}_i)$  in (5) would naturally converge to the solution.

#### A. Conditions for Optimal Point in ANM

The solution to the AST problem (2) must satisfy the following conditions [11, Lemma 1]:

**Lemma 1:** Let  $\mathbf{x}^*$  be the solution to the optimization problem (2). Then  $\mathbf{x}^*$  must satisfy: (i)  $\sup_{\mathbf{a} \in \mathcal{A}} \langle \mathbf{y} - \mathbf{x}^*, \mathbf{a} \rangle \leq \zeta^{-1}$  (ii)  $\langle \mathbf{x}^*, \mathbf{y} - \mathbf{x}^* \rangle = \zeta^{-1} \|\mathbf{x}^*\|_{\mathcal{A}}$ .

Let  $\mathbf{z}^* = \mathbf{y} - \mathbf{x}^*$  be the residual of  $\mathbf{y}$  in the solution.  $\mathbf{z}^*$  is also known as the dual certificate of support as it indicates the elements  $\mathbf{a}_i$  in the sparse representation of  $\mathbf{x}^*$ . In Lemma 1, if the solution  $\mathbf{x}^*$  is non-trivial, i.e.,  $\mathbf{x}^* \neq \mathbf{0}$ , then the inequality in (i) is tight. Consequently, there exists elements  $\mathbf{a}_i \in \mathcal{A}$  such that  $\langle \mathbf{y} - \mathbf{x}^*, \mathbf{a}_i \rangle = \zeta^{-1}$ . Let  $\mathcal{S}$  be the set of all such elements. The solution  $\mathbf{x}^*$  then admits a decomposition over  $\mathcal{S}$ :  $\mathbf{x}^* = \sum_i c_i \mathbf{a}_i, \mathbf{a}_i \in \mathcal{S}$  [2]. It is not hard to see that such a decomposition of  $\mathbf{x}^*$  is unique due to the existence of the dual certificate  $\mathbf{z}^*$  [11, Corollary 1]. In a typical use case of ANM such as direction of arrival (DoA) estimation [18], the elements  $\mathbf{a}_i \in \mathcal{S}$  typically reveals the values of the estimated parameter from its continuous domain.

With the notion of the dual polynomial, the equivalence between (2) and (5) can be readily shown. The main idea is that the solution  $\mathbf{x}^*$  is represented by a set of tuples  $(c_i, \mathbf{a}_i)$ . The residual  $\mathbf{z}^* = \mathbf{y} - \mathbf{x}^*$  has the maximum inner product with the elements  $\mathbf{a}_i$  in  $\mathcal{S}$ , i.e.,  $\langle \mathbf{z}^*, \mathbf{a}_i \rangle = \zeta^{-1}$ . In the mixed integer formulation, the residual  $\mathbf{y} - \sum_i^L c_i \mathbf{a}_i$  is the dual polynomial:

**Lemma 2:** Suppose  $\mathcal{A}$  is symmetric with respect to the origin. Let  $(c_1, \mathbf{a}_1), (c_2, \mathbf{a}_2), \dots, (c_L, \mathbf{a}_L)$  be the global optimal point to the mixed integer problem (5) such that  $c_i > 0, \mathbf{a}_i \in \mathcal{A}$ . Then the residual  $\mathbf{y}_r = \mathbf{y} - \sum_i^L c_i \mathbf{a}_i$  must satisfy the inequality:  $\sup_{\mathbf{a} \in \mathcal{A}} \langle \mathbf{y}_r, \mathbf{a} \rangle \leq \zeta^{-1}$ .

*Proof:* The proof is straightforward. The key is to consider a function  $f(\mathbf{x}, \mathcal{A}, \zeta)$  defined as following:

$$\begin{aligned} f(\mathbf{x}, \mathcal{A}, \zeta) &= \inf_{c \geq 0, \mathbf{a} \in \mathcal{A}} \frac{\zeta}{2} \|\mathbf{x} - c\mathbf{a}\|_2^2 + c \quad (10) \\ &= \frac{\zeta}{2} \|\mathbf{x}\|_2^2 + \inf_{c \geq 0, \mathbf{a} \in \mathcal{A}} c(1 - \zeta \langle \mathbf{x}, \mathbf{a} \rangle) + \frac{c^2 \zeta}{2} \|\mathbf{a}\|_2^2 \\ &\leq \frac{\zeta}{2} \|\mathbf{x}\|_2^2 \end{aligned}$$

Notice that (10) contains a shrinkage and thresholding operation. When the inequality  $\sup_{\mathbf{a} \in \mathcal{A}} \langle \mathbf{x}, \mathbf{a} \rangle \leq \zeta^{-1}$  holds,  $f(\mathbf{x}, \mathcal{A}, \zeta) = \frac{\zeta}{2} \|\mathbf{x}\|_2^2$ . It's straight forward to see that the reverse statement is also true. If  $f(\mathbf{x}, \mathcal{A}, \zeta) = \frac{\zeta}{2} \|\mathbf{x}\|_2^2$ , there must be  $\sup_{\mathbf{a} \in \mathcal{A}} \langle \mathbf{x}, \mathbf{a} \rangle \leq \zeta^{-1}$ .

Since the set of tuples  $(c_i, \mathbf{a}_i), i = 1, \dots, L$  is the global optimal point, its objective value must be the global minimum. Therefore, adding one more tuple  $(c_0, \mathbf{a}_0)$  to the set can only increase the objective value. This results in the following inequality:

$$\begin{aligned} \sum_{i=1}^L c_i + \frac{\zeta}{2} \|\mathbf{y}_r\|_2^2 &\leq \inf_{c_0 \geq 0, \mathbf{a}_0 \in \mathcal{A}} \sum_{i=0}^L c_i + \frac{\zeta}{2} \|\mathbf{y}_r - c_0 \mathbf{a}_0\|_2^2 \\ &= \sum_{i=1}^L c_i + f(\mathbf{y}_r, \mathcal{A}, \zeta) \\ &\leq \sum_{i=1}^L c_i + \frac{\zeta}{2} \|\mathbf{y}_r\|_2^2 \end{aligned}$$

It's trivial to see that  $f(\mathbf{y}_r, \mathcal{A}, \zeta) = \frac{\zeta}{2} \|\mathbf{y}_r\|_2^2$ , which means  $\sup_{\mathbf{a} \in \mathcal{A}} \langle \mathbf{y}_r, \mathbf{a} \rangle \leq \zeta^{-1}$ . ■

Lemma 2 points out that in the solution of (5) the residual  $\mathbf{y}_r$  must satisfy the condition (i) in Lemma 1. It remains to show that condition (ii) should also be satisfied. Condition (ii) is a consequence of the fact that each tuple  $(c_i, \mathbf{a}_i)$  in the solution must also be a stationary point. Let  $h$  be the objective function in (5), i.e.,

$$h(c_1, \mathbf{a}_1, \dots, c_L, \mathbf{a}_L) = \sum_{i=1}^L c_i + \frac{\zeta}{2} \left\| \mathbf{y} - \sum_{i=1}^L c_i \mathbf{a}_i \right\|_2^2 \quad (11)$$

Since each tuple is a stationary point of  $h$ , their partial derivative must be 0. Specifically, let  $\mathbf{y}_r^i = \mathbf{y}_r + c_i \mathbf{a}_i$ . The

following condition on partial derivative must be satisfied:

$$\begin{aligned}\frac{\partial h}{\partial c_i} &= \frac{\partial}{\partial c_i} \left( \frac{\zeta}{2} \|\mathbf{y}_r^i - c_i \mathbf{a}_i\|_2^2 + \sum_{j=1}^L c_j \right) \\ &= -\zeta \langle \mathbf{a}_i, \mathbf{y}_r^i - c_i \mathbf{a}_i \rangle + 1 \\ &= 0\end{aligned}\quad (12)$$

Which implies that:

$$\langle \mathbf{a}_i, \mathbf{y}_r^i \rangle - \zeta^{-1} = c_i \|\mathbf{a}_i\|_2^2 \quad (13)$$

Now notice that previously it is defined such that:  $\mathbf{y}_r^i = \mathbf{y}_r + c_i \mathbf{a}_i$ . Therefore, by plugging in the definition of  $\mathbf{y}_r$  into (13),

$$\langle \mathbf{a}_i, \mathbf{y}_r \rangle = \zeta^{-1} \quad (14)$$

**Remark 1:** (14) proves the indicating property of the dual polynomial. Together with lemma (2), it's not hard to see that  $\mathbf{y}_r$  has the maximum inner product  $\langle \mathbf{y}_r, \mathbf{a} \rangle = \zeta^{-1}$  with  $\mathbf{a} \in \mathcal{A}$  if  $\mathbf{a}$  is part of the solution. Using this property, the equivalence between (2) and (5) can be readily established.

**Theorem 1:** Suppose  $\mathcal{A}$  is symmetric with respect to the origin. Let  $(c_1, \mathbf{a}_1), (c_2, \mathbf{a}_2), \dots, (c_L, \mathbf{a}_L)$  be the global optimal point to the mixed integer problem (5) such that  $c_i > 0, \mathbf{a}_i \in \mathcal{A}$ . Then  $\mathbf{x} = \sum_i^L c_i \mathbf{a}_i$  is also the solution to the ANM problem (2) and  $\|\mathbf{x}\|_{\mathcal{A}} = \sum_i^L c_i$ .

*Proof:* With Lemma 2, the first condition in 1 has been proved to be satisfied by the set of tuples  $(c_i, \mathbf{a}_i)$ . To show that the second condition is also satisfied by  $\mathbf{x} = \sum_i^L c_i \mathbf{a}_i$ , the first step is to use the property (14). Notice that:

$$\langle \mathbf{y} - \mathbf{x}, \mathbf{x} \rangle = \sum_i^L c_i \langle \mathbf{y}_r, \mathbf{a}_i \rangle = \frac{1}{\zeta} \sum_{i=1}^L c_i \quad (15)$$

It remains to show that  $\sum_i^L c_i = \|\mathbf{x}\|_{\mathcal{A}}$ . Since the set of tuples is the global optimal point that solves (5), it must satisfy the definition (4), i.e.,  $\sum_i^L c_i = \|\mathbf{x}\|_{\mathcal{A}}$  must hold. Consequently,  $\mathbf{x} = \sum_i^L c_i \mathbf{a}_i$  satisfies both the conditions of optimality for (2) in Lemma 1. This concludes the proof. ■

**Remark 2:** A major part of the proof for theorem 1 relies on the assumption that the set of tuples  $(c_i, \mathbf{a}_i)$  is the global optimal point. In fact, it has been proved previously [11, Corollary 1] such that once the residual  $\mathbf{y}_r = \mathbf{y} - \mathbf{x}$  satisfies the two conditions of being a dual certificate, namely,  $\langle \mathbf{y}_r, \mathbf{a} \rangle \leq \zeta^{-1}$  and (14), then  $\|\mathbf{x}\|_{\mathcal{A}} = \sum_{i=1}^L c_i$  must hold which in turn makes the set global optimal. For readers' convenience, an outline of the proof is provided here. Instead of assuming  $(c_1, \mathbf{a}_1), (c_2, \mathbf{a}_2), \dots, (c_L, \mathbf{a}_L)$  is the global optimal set, let's assume that  $\mathbf{y}_r = \mathbf{y} - \sum_{i=1}^L c_i \mathbf{a}_i$  satisfies the two conditions, namely,  $\sup_{\mathbf{a} \in \mathcal{A}} \langle \mathbf{y}_r, \mathbf{a} \rangle \leq \zeta^{-1}$  and  $\langle \mathbf{y}_r, \mathbf{a}_i \rangle = \zeta^{-1}, i = 1, 2, \dots, L$ . Consequently, there is still  $\langle \mathbf{y}_r, \mathbf{x} \rangle = \zeta^{-1} \sum_i^L c_i$ . Now suppose  $\|\mathbf{x}\|_{\mathcal{A}} < \sum_i^L c_i$  which implies that  $\mathbf{x}$  admits a different decomposition  $\mathbf{x} = \sum_i^{L'} c'_i \mathbf{a}'_i$  such that  $\sum_i^{L'} c'_i = \|\mathbf{x}\|_{\mathcal{A}} < \sum_i^L c_i$ . A conflict is readily established:

$$\langle \mathbf{y}_r, \mathbf{x} \rangle = \sum_i^{L'} c'_i \langle \mathbf{y}_r, \mathbf{a}'_i \rangle \leq \zeta^{-1} \sum_i^{L'} c'_i < \zeta^{-1} \sum_i^L c_i = \langle \mathbf{y}_r, \mathbf{x} \rangle \quad (16)$$

It's not hard to see that the dual certificate  $\mathbf{y}_r$  ensures that  $\|\mathbf{x}\|_{\mathcal{A}} = \sum_i^L c_i$ .

From theorem 1, the equivalence between the two formulation of ANM is established. Additionally, remark 2 actually provides the two conditions required for a set of tuples to be the solution to the mixed-integer problem (5). The next subsection introduces a practical algorithm to solve (5) based on these conditions. Consequently, the algorithm simultaneously solves the original ANM problem (2).

### B. Algorithmic Framework for ANM

Theorem 1 provides a simple but critical perspective for solving ANM: the global optimal solution is found once a set of tuples is properly chosen such that the two conditions of being a dual certificate are satisfied by the residual. The remaining question is then how to choose such a set of tuples  $(c, \mathbf{a})$ . Inspired by previous work on applying the coordinate descent to (1) [14], [15], a similar iterative strategy can be developed for (5). Reusing the notations in (11) - (14), let's assume in the  $k$ -th iteration, there are  $L_k$  tuples in the set. The main algorithmic steps are generically stated as:

- In the  $k$ -th iteration, if a tuple  $(c_i, \mathbf{a}_i)$  from the current set  $(c_1, \mathbf{a}_1), \dots, (c_{L_k}, \mathbf{a}_{L_k})$  is chosen, the tuple is refined by solving a coordinate descent step on  $\mathbf{y}_r^i = \mathbf{y}_r + c_i \mathbf{a}_i$ :

$$\begin{aligned}(c_i, \mathbf{a}_i) &= \operatorname{argmin}_{c \geq 0, \mathbf{a} \in \mathcal{A}} h(c_1, \mathbf{a}_1, \dots, c, \mathbf{a}, \dots, c_{L_k}, \mathbf{a}_{L_k}) \\ &= \operatorname{argmin}_{c \geq 0, \mathbf{a} \in \mathcal{A}} \frac{\zeta}{2} \|\mathbf{y}_r^i - c\mathbf{a}\|_2^2 + c\end{aligned}\quad (17)$$

If in the result  $c_i = 0$ , the tuple is removed from the current set.

- In the  $k$ -th iteration, if no tuple from the current set is chosen, then the conditions on whether  $\mathbf{y}_r$  is a valid dual certificate should be checked. If  $\sup_{\mathbf{a} \in \mathcal{A}} \langle \mathbf{y}_r, \mathbf{a} \rangle > \zeta^{-1}$ , a new tuple  $(c_{L_k+1}, \mathbf{a}_{L_k+1})$  should be added to the current set. The new tuple should be obtained by also a coordinate descent step on  $\mathbf{y}_r$ :

$$(c_{L_k+1}, \mathbf{a}_{L_k+1}) = \operatorname{argmin}_{c \geq 0, \mathbf{a} \in \mathcal{A}} \frac{\zeta}{2} \|\mathbf{y}_r - c\mathbf{a}\|_2^2 + c \quad (18)$$

On the other hand if both (i)  $\sup_{\mathbf{a} \in \mathcal{A}} \langle \mathbf{y}_r, \mathbf{a} \rangle \leq \zeta^{-1}$  and (ii)  $\langle \mathbf{y}_r, \mathbf{y} - \mathbf{y}_r \rangle = \zeta^{-1} \sum_i^{L_k} c_i$  hold, the algorithm terminates.

The procedure above does not have the strategy for choosing one tuple from the set. In fact, such a strategy can be customized to be greedy, cyclic, or simply random. As an example, a pseudo for cyclic coordinate descent applying to ANM initialized with an empty set is given in algorithm 1.

Besides its cyclic sampling strategy, algorithm 1 exemplifies several key features of the proposed coordinate descent framework for ANM. First, it is essentially matrix-free. Throughout the iterations, only the set of tuples  $\mathcal{S}$ , the residual vector  $\mathbf{y}_r$ , and the original vector  $\mathbf{y}$  are being stored. Second, in each iteration the relatively expensive steps are refinements (line 7 or line 15) or checking the condition of the if statements (line 14). All other steps have only  $\mathcal{O}(N)$  computational complexity. As it will be illustrated later, for the classical

---

**Algorithm 1** Cyclic Coordinate Descent for ANM

---

1: **Input:**  
Observation vector  $\mathbf{y}$ ; Atomic set  $\mathcal{A}$ ; Threshold  $\zeta$ ;  
Tolerance  $\text{tol}$ ; Maximum Iteration  $M$ ;

2: **Initialize:**  
Empty set of tuples  $\mathcal{S}$ ; Residual vector  $\mathbf{y}_r \leftarrow \mathbf{y}$ ;  
 $L \leftarrow 0, i \leftarrow 1$ ;

3: **for**  $k = 1, 2, \dots, M$  **do**

4:   **if**  $i \leq L$  **then**

5:      $(c_i, \mathbf{a}_i) \leftarrow [\mathcal{S}]_i$

6:      $\mathbf{y}_r^i \leftarrow \mathbf{y}_r + c_i \mathbf{a}_i$

7:      $(c_i, \mathbf{a}_i) \leftarrow \underset{c \geq 0, \mathbf{a} \in \mathcal{A}}{\text{argmin}} \frac{\zeta}{2} \|\mathbf{y}_r^i - c\mathbf{a}\|_2^2 + c$

8:      $\mathbf{y}_r \leftarrow \mathbf{y}_r^i - c_i \mathbf{a}_i, [\mathcal{S}]_i \leftarrow (c_i, \mathbf{a}_i)$

9:     **if**  $c_i == 0$  **then**

10:       Remove  $(c_i, \mathbf{a}_i)$  from  $\mathcal{S}, L \leftarrow L - 1, i \leftarrow i - 1$

11:     **end if**

12:      $i \leftarrow i + 1$

13:   **else if**  $\left| \sum_j^L c_j - \zeta \langle \mathbf{y}_r, \mathbf{y} - \mathbf{y}_r \rangle \right| \leq \text{tol}$  **then**

14:     **if**  $\sup_{\mathbf{a} \in \mathcal{A}} \langle \mathbf{y}_r, \mathbf{a} \rangle > \zeta^{-1}$  **then**

15:        $(c_{L+1}, \mathbf{a}_{L+1}) = \underset{c \geq 0, \mathbf{a} \in \mathcal{A}}{\text{argmin}} \frac{\zeta}{2} \|\mathbf{y}_r - c\mathbf{a}\|_2^2 + c$

16:        $\mathbf{y}_r \leftarrow \mathbf{y}_r - c_{L+1} \mathbf{a}_{L+1}$

17:       Add  $(c_{L+1}, \mathbf{a}_{L+1})$  to  $\mathcal{S}, L \leftarrow |\mathcal{S}|, i \leftarrow 1$

18:     **else**

19:       **Break**

20:     **end if**

21:   **else**

22:      $i \leftarrow 1$

23:   **end if**

24: **end for**

25: **return** The set of tuples  $\mathcal{S}$ , Residual  $\mathbf{y}_r$

---

atomic set (6), these steps have only  $\mathcal{O}(N \log N)$  operations. In addition, with large enough  $M$ , the algorithm is guaranteed to converge. It's not hard to see that in each iteration, the value of the objective function  $h$  in (11) strictly decreases. Upon convergence, the set  $\mathcal{S}$  must be stationary which indicates that  $\mathcal{S}$  is optimal.

**Remark 3:** So far in algorithm 1, it is not required that different tuples from  $\mathcal{S}$  must have different elements from  $\mathcal{A}$ . Although the solution  $\mathbf{x}$  to (2) is unique, the optimal set that solves (5) is not be unique unless it is restricted that different tuples must have different elements from  $\mathcal{A}$ , i.e.,  $\mathbf{a}_i \neq \mathbf{a}_j$  if  $i \neq j$ . Therefore upon convergence of algorithm 1, multiple tuples in  $\mathcal{S}$  might have the same element from  $\mathcal{A}$ . Such ambiguities do not prevent the algorithm from convergence.

In general, the complexity of solving (17) or (18) as well as calculating  $\sup_{\mathbf{a} \in \mathcal{A}} \langle \mathbf{y}_r, \mathbf{a} \rangle$  depends on the structure of  $\mathcal{A}$ . The rest of this section addresses these two operations for  $\mathcal{A}$  defined as in (6). The calculation can be easily generalized to atomic sets in (8), (7). With this choice of  $\mathcal{A}$ , the vector space of interests is  $\mathbb{C}^N$  with the inner-product defined as  $\langle \mathbf{x}, \mathbf{y} \rangle = \text{Re} \{ \mathbf{x}^H \mathbf{y} \}$ .

With the derivation in (10) and the definition (6), (18) is

equivalent to the following optimization problem:

$$\begin{aligned} \underset{\phi, f, c}{\text{Minimize}} \quad & c \left( 1 - \zeta \langle \mathbf{y}_r, e^{1j\phi} \mathbf{a}(f) \rangle \right) + \frac{Nc^2\zeta}{2} \quad (19) \\ \text{subject to} \quad & c \geq 0; \phi, f \in [0, 2\pi); \end{aligned}$$

Let  $c^*, f^*, \phi^*$  be the solution. The problem has a separable structure:

$$f^* = \underset{f}{\text{argmax}}_f |\mathbf{y}_r^H \mathbf{a}(f)| \quad (20)$$

$$c^* = \begin{cases} 0, & |\mathbf{y}_r^H \mathbf{a}(f^*)| \leq \frac{1}{\zeta} \\ \frac{1}{N} \left( |\mathbf{y}_r^H \mathbf{a}(f^*)| - \frac{1}{\zeta} \right), & |\mathbf{y}_r^H \mathbf{a}(f^*)| > \frac{1}{\zeta} \end{cases} \quad (21)$$

$$\phi^* = -\angle(\mathbf{y}_r^H \mathbf{a}(f^*)) \quad (22)$$

It's straight forward to see that the key step is (20). As a consequence, solving (17) or (18) is almost the same as evaluating  $\sup_f |\langle \mathbf{y}_r, \mathbf{a}(f) \rangle|$  in (20). The problem is essentially locating the maximum of a polynomial on the unit circle.<sup>2</sup> For this purpose, the low-complexity approach in NOMP [17] can be employed:

---

**Algorithm 2** Calculating the Maximum on the Unit Circle

---

1: **Input:**  
Complex vector  $\mathbf{y} \in \mathbb{C}^N$ ; Tolerance  $\text{tol} = 10^{-12}$ ;  
Oversampling Ratio  $r = 16$

2: **Initialize:**  
Construct  $\hat{\mathbf{y}} \in \mathbb{C}^{2N}$  such that:  
 $[\hat{\mathbf{y}}]_{1:N} = \mathbf{y}, [\hat{\mathbf{y}}]_{N+1:2N} = \mathbf{0}$

3:  $\tilde{\mathbf{y}} \leftarrow \left[ \mathcal{F}^{-1} |\mathcal{F} \{ \hat{\mathbf{y}} \}|^2 \right]_{1:2N}$

4: Evaluate  $\text{Re} \{ \tilde{\mathbf{y}}^H \mathbf{a}(f) \}$  on an uniform grid of  $rN$  points  $f = 0, \frac{2\pi}{rN}, \dots, \frac{2\pi(rN-1)}{rN}$  using FFT

5:  $f^* \leftarrow$  the on-grid point with the largest  $\text{Re} \{ \tilde{\mathbf{y}}^H \mathbf{a}(f) \}$  among these  $rN$  points

6: **while True do**

7:    $\Delta f \leftarrow \text{Re} \{ \tilde{\mathbf{y}}^H \nabla_f \mathbf{a}(f^*) \} / \text{Re} \{ \tilde{\mathbf{y}}^H \nabla_f^2 \mathbf{a}(f^*) \}$

8:   **if**  $\Delta f \leq \text{tol}$  **then**

9:     **Break**

10:   **end if**

11:    $f^* \leftarrow f^* - \Delta f$

12: **end while**

13: **return**  $f^*$  such that  $|\mathbf{y}^H \mathbf{a}(f^*)|^2 = \sup_f |\mathbf{y}^H \mathbf{a}(f)|^2$

---

With FFT, algorithm 2 has  $\mathcal{O}(N \log N)$  operations. Specifically, the initialization steps line 2 and line 3 calculate  $\tilde{\mathbf{y}}$  such that  $\text{Re} \{ \tilde{\mathbf{y}}^H \mathbf{a}(f) \} = |\mathbf{y}^H \mathbf{a}(f)|^2$ . Line 4 and line 5 then perform initial over sampling on an uniform grid. Line 6 to line 12 have only  $\mathcal{O}(N)$  operations. These steps use Newton's method to calculate the off-grid maximum of the function  $\text{Re} \{ \tilde{\mathbf{y}}^H \mathbf{a}(f) \}$ . It has been shown previously that  $r > 1$  is necessary to ensure the convergence to the true maximum as the function  $\text{Re} \{ \tilde{\mathbf{y}}^H \mathbf{a}(f) \}$  on the interval  $[0, 2\pi)$  is non-convex. The default value  $r = 16$  is established empirically<sup>3</sup>

<sup>2</sup>Note that the algorithm 2 have specific steps designed for the simple set (6). The coordinate descent framework algorithm 1 on the other hand applies to general atomic sets.

<sup>3</sup>A rigorous discussion on how large  $r$  should be is related to the spacing between roots of a polynomial on the unit circle, which is beyond the scope.

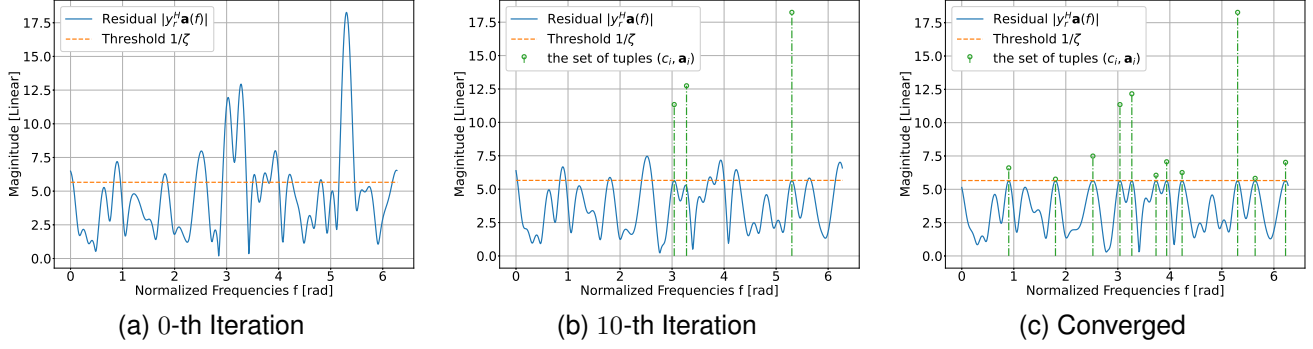


Fig. 1: Visualization of convergence in randomized coordinate descent. Through iterations, tuples  $(c_i, \mathbf{a}_i)$  are added to the set  $\mathcal{S}$ . Each red stem in the plot represents an element  $\mathbf{a}_i$  with corresponding scaling  $c_i + 1/\zeta$  in the tuple. With 10 iterations, only 3 tuples are added to  $\mathcal{S}$ . At convergence, there are total 11 tuples in  $\mathcal{S}$ .

and is found to be sufficient in this work. It is also independent from the size of the problem  $N$ . Algorithm 2 provides a low-complexity method to check whether the condition in line 18 in algorithm 1 holds. With (20) - (22), it also solves (17) or (18). With the missing pieces sorted out by algorithm 2, algorithm 1 is readily applicable to ANM problems with the atomic set (6).

Figure 1 provides visualizations for the convergence of algorithm 1 on an exemplary problem in which  $N = 32$ ,  $\mathbf{y} \in \mathbb{C}^{32}$ . Each entry  $[y]_i$  is independently sampled from  $\mathcal{CN}(0, 1)$ . The parameter  $\zeta$  is set to  $\zeta = 1/\sqrt{N} = 1/\sqrt{32}$ . The algorithm converges at 967-th iterations with duality gap smaller than  $\text{tol} = 10^{-12}$ .

### C. Generic Acceleration Techniques

Before evaluating the performance of the proposed algorithm, this section introduces a generic technique that can speed up the convergence of the proposed algorithm. The major weakness of algorithm 1 is the rate of convergence. In previous works on block coordinate descent algorithms applied to LASSO problems, a linear convergence rate has been established [19], as the problem (1) is smooth and convex. The linear rate of convergence for LASSO is observed numerically even when matrix  $\mathbf{A}$  is badly conditioned. Otherwise, for general non-smooth problems, the worst-case rate of convergence of coordinate descent is sub-linear [20].

From a theoretical perspective, it is hard to establish similar results for the mixed integer problem (5), as the number of coordinates  $L$  is changing throughout iterations. From a practical perspective, a linear convergence rate is only observed when the set  $\mathcal{S}$  is nearly optimal and no new tuple  $(c, \mathbf{a})$  is added. At this stage, (5) becomes very similar to the LASSO problem (1) as in each tuple  $(c_i, \mathbf{a}_i)$  the element  $\mathbf{a}_i$  almost converges. Therefore, the technique discussed in this section is designed generically to quickly get to the stage that has a linear rate of convergence. In algorithm 1, a new tuple would only be added if the if statement in line 13 is satisfied. The main idea here is to prevent the set  $\mathcal{S}$  from growing too quickly. However, it also introduces unnecessary iterations as the high precision is not needed for new atoms to be added.

The unnecessary iterations can be reduced by calling algorithm 1 twice in which the result from the first call is used to initialize the second call as a warm start. The first call uses a larger tolerance (e.g.,  $\text{tol} = 10^{-6}$ ) and the second call uses the desired precision (e.g.,  $\text{tol} = 10^{-12}$ ). The initialization steps (line 2) in algorithm 1 can be easily altered to accommodate non-empty set  $\mathcal{S}$ . A comparison of the rates between the two-step approach and the direct approach is provided in figure 2. The problem being solved has the same  $\zeta = 1/\sqrt{N} = 1/\sqrt{32}$  as that of figure 1 but a different sampled vector  $\mathbf{y}$ . As predicted, solving the problem with a relaxed tolerance first allows tuples to be added quickly to  $\mathcal{S}$ , after which a linear convergence rate is established.

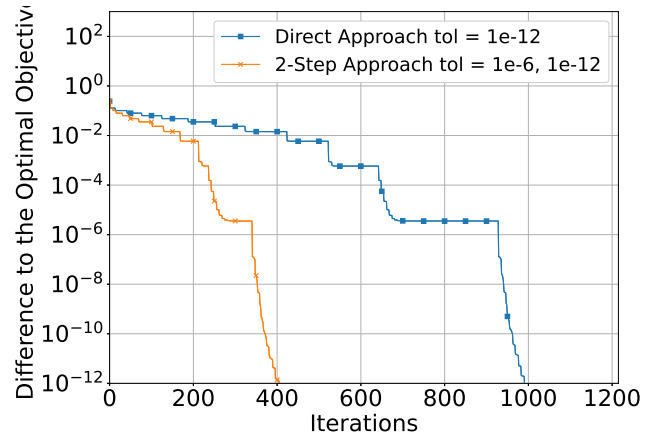


Fig. 2: Visualization of convergence in cyclic coordinate descent. The  $y$ -axis characterizes the sub-optimality of the current iteration. The two-step strategy saves approximately half of the iterations.

This concludes the discussion on algorithmic development of the proposed approach. In fact, the method can be further customized (for instance, with different initial set  $\mathcal{S}$ ). In particular, the strategy of a solution path [15] has also been tried but does not yield significant improvement on the speed of convergence. The next section provides numerical experiments that showcase the performances of the coordinate descent approach on various ANM example problems.

#### IV. NUMERICAL EXPERIMENTS

In this section, a series of numerical examples are presented to demonstrate the strength and weakness of the proposed method. Due to the space limit, relevant derivations on how problem (10) maps for different atomic sets  $\mathcal{A}$  are included in the Appendix.

##### A. Time Trials

To demonstrate the efficiency of the proposed method, a sequence of sparse ANM problems are constructed. The value  $\zeta = (N \log N / 4)^{-1/2}$  is used for  $N = \{32, 64, 128, 256, 1024, 2048, 4096\}$  in which each entry of  $\mathbf{y} \in \mathbb{C}^N$  is again sampled from circularly symmetric Gaussian random distribution. The atomic set  $\mathcal{A}$  is defined as in (6). Let  $L_{\min}$  be the minimum number of tuples in the solution to (5). The parameter  $\zeta$  controls the level of sparsity for the underlying ANM problems. Specifically in this experiment, the case  $\zeta = (N \log N / 4)^{-1/2}$  yields  $L_{\min} \leq 20$  for all  $N$  with high probability regardless of  $N$ .

The ADMM solver and the SOTA interior-point solver from [5] are employed for comparison. They're downloaded directly from the author's original repository on Github [21]. The mexfile in the implementation is then built and executed in MATLAB 2020b [22]. On the other hand, the coordinate descent method is implemented in CPP with libraries FFTW v3.3.10 and Eigen v3.4.1 with a Python wrapper. The results of the time trials are provided in figure 3. For the interior point and the ADMM solver, each data point is an average over 20 Monte Carlo trials. For the coordinate descent method, each point is an average over 200 trials.

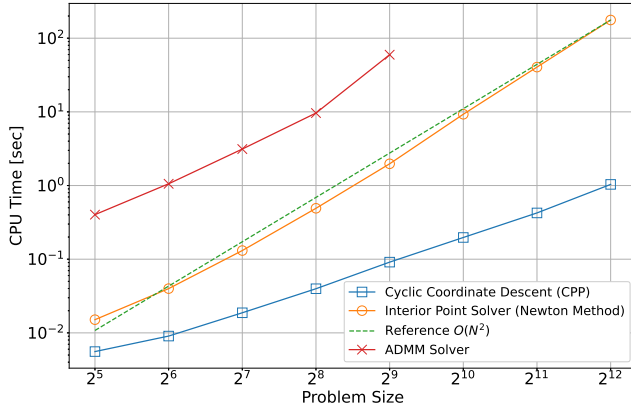


Fig. 3: Time Trials on sparse ANM problems.

In practice, it is found that for sparse ANM problems, the interior-point solver with fast implementation for solving Toeplitz linear systems has  $\mathcal{O}(N^2)$  complexity regardless of  $L_{\min}$ , whereas the complexity of the proposed method has  $\mathcal{O}(L_{\min}^2 N \log(N))$  behavior. As indicated in figure 3, when  $L_{\min} \ll N$ , the proposed method has a clear advantage over the SOTA interior-point method.

Moreover, the strength of the proposed method is not only its efficiency on sparse problems but also its flexibility. Note that the fast computations on Toeplitz linear system which make the SOTA interior-point method behave like  $\mathcal{O}(N^2)$

are only implemented for the simplest DFT atomic set (6). No other atomic set  $\mathcal{A}$  was addressed in [5]. In fact, using the SOTA interior point method to solve more generalized ANM problems is hard as the evaluation of Hessian is complicated. The coordinate descent framework, however, can be generalized easily. In the next subsection, several numerical experiments with different atomic set  $\mathcal{A}$  will be presented.

##### B. Application to MMV ANM with 2D Frequencies

It is well known that ANM problems with MMV (with atomic set (7)) or with two-dimensional frequencies (with atomic set (8)) can be decoupled [7], [23]. Decoupling is to formulate the SDP constraint smartly such that the size of the problem is  $N + M$  instead of  $NM + 1$  in the case of (7) with  $M$  samples, or is  $N + N$  instead of  $N^2 + 1$  in the case of (8) with both DFT vectors of length  $N$ . However, due to the limitation of the bounded real lemma, decoupling ANM problems with two-dimensional DFT set and MMV is not a trivial task. To the best of our knowledge, [8] is the SOTA along this direction. However, in [8] the authors resorted to the construction of a covariance matrix with redundancy reduction. Although this technique reduces the complexity of the problem, it also loses the robustness with respect to the correlation among signal sources. And to ensure the quality of the covariance construction, a large number of samples (for instance,  $M \geq 200$ ) are needed.

Without decoupling, the complexity of solving a two-dimensional MMV ANM problem in the SDP formulation is about  $\mathcal{O}((N^2 + M)^3)$ . Such high complexity can be easily reduced with the proposed coordinate descent framework. Let  $\mathbf{Y} \in \mathbb{C}^{N \times N \times M}$  be the tensor of interest. The two-dimensional MMV ANM problem can be equivalently formulated as:

$$\text{Minimize}_{L, \mathbf{c}_i \in \mathbb{C}^M, f_i^1, f_i^2} \sum_i \|\mathbf{c}_i\|_2 + \frac{\zeta}{2} \left\| \mathbf{Y} - \sum_i \mathbf{a}(f_i^1) \otimes \mathbf{a}(f_i^2) \otimes \mathbf{c}_i \right\|_2^2 \quad (23)$$

It not hard to see that (23) can be solved by the framework in algorithm 1. With the help of two-dimensional FFT the complexity of one iteration in the coordinate descent algorithm is only  $\mathcal{O}(M(N \log N)^2)$ . The key step is still solving a sub problem similar to (18):

$$\text{Minimize}_{\mathbf{c}_i \in \mathbb{C}^M, f_i^1, f_i^2} \|\mathbf{c}_i\|_2 + \frac{\zeta}{2} \left\| \mathbf{Y}_r - \mathbf{a}(f_i^1) \otimes \mathbf{a}(f_i^2) \otimes \mathbf{c}_i \right\|_2^2 \quad (24)$$

subject to  $f_i^1, f_i^2 \in [0, 2\pi)$ ;

To keep the discussion relevant, details on solving (24) using the method similar to algorithm 2 are presented in appendix. To demonstrate the effectiveness of the proposed method, an ANM scenario of  $N = 32, M = 5$  is simulated. Specifically, the tensor of interest  $\mathbf{Y} \in \mathbb{C}^{32 \times 32 \times 5}$  is generated from the following:

$$\mathbf{Y} = \sum_{i=1}^L \mathbf{a}(f_i^1) \otimes \mathbf{a}(f_i^2) \otimes \mathbf{c}_i + \mathbf{N} \quad (25)$$

Each entry of  $\mathbf{N} \in \mathbb{C}^{32 \times 32 \times 5}$  is sampled from standard circularly symmetric Gaussian random distribution. All signal



tensors have the same power, i.e.,  $\|\mathbf{c}_i\|_2 = P$ . The angles  $f_i^1, f_i^2$  are independently randomly sampled from uniform distribution over the interval  $[0, 2\pi)$ . Let  $N_1 = N_2 = N$ . Inspired by the derivation in [11], a heuristic value of  $\zeta$  is used:

$$\zeta = \left(\frac{\ln M}{M}\right)^{1/2} (N_1 N_2 \ln(N_1 N_2 \ln N_1 N_2 + 1))^{-1} \quad (26)$$

In this experiment,  $1/\zeta = 139.14$  is calculated from  $N_1 = N_2 = 32, M = 5$ . In every trial,  $\mathbf{Y}$  is generated with  $L = 16$  signal tensors. After running ANM on  $\mathbf{Y}$ , the estimated angles  $\hat{f}_i^1, \hat{f}_i^2$  from the set  $\mathcal{S}$  are compared with the ground truth. A visualization of the spectrum of the residual tensor  $\|\langle \mathbf{Y}_r, \mathbf{a}(f_1) \otimes \mathbf{a}(f_2) \rangle\|_2$  is provided in the figure 4.  $\mathbf{Y}_r$  is the second output from algorithm 1. As in typical ANM problems, the residual tensor  $\mathbf{Y}_r$  demonstrates the typical behavior of a dual polynomial. Its spectrum indicates the true frequencies.

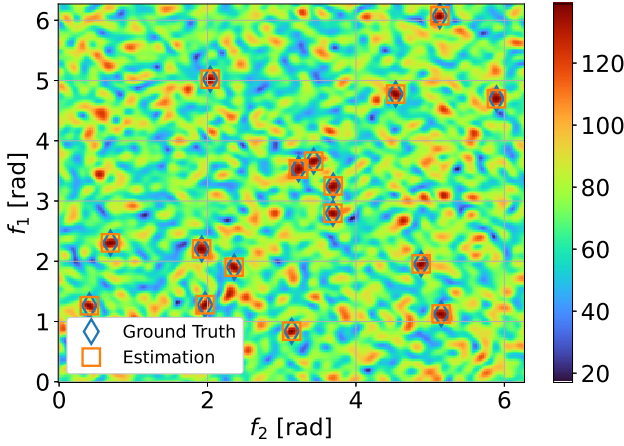


Fig. 4: Visualization of the spectrum of a residual tensor  $\mathbf{Y}_r \in \mathbb{C}^{32 \times 32 \times 5}$  in a random trial. With two-dimensional and MMV observations, even clustered sources can be differentiated.

The signal-to-noise ratio (SNR) per signal tensor in this experiment is calculated as  $\text{SNR} = 20 \log_{10}(\frac{P}{M})$ . The error in the estimation process is calculated as:

$$\Delta = \sqrt{\left(\hat{f}_i^1 - f_i^1\right)^2 + \left(\hat{f}_i^2 - f_i^2\right)^2} \quad (27)$$

The results are compared with the corresponding Cramér–Rao bound (CRB) in figure 5. CRB in this experiment is calculated from the standard approach in [17, Appendix II]. Similar to results from previous work, the proposed coordinate descent algorithm delivers the same level of accuracy as that of other solvers for ANM problems.

### C. Application to weighted ANM

A major weakness of ANM with DFT atomic sets (6) is the separation requirement. It has been proven that in order for two distinct elements  $\mathbf{a}(f_1), \mathbf{a}(f_2) \in \mathbb{C}^N$  to be identified in ANM with high probability, the difference between their frequencies must be large enough  $|f_1 - f_2| \geq \frac{4}{N}$  [2], [3], [24]. To overcome such a requirement, a weighted ANM scheme is proposed in [25]. The main idea is that instead of using

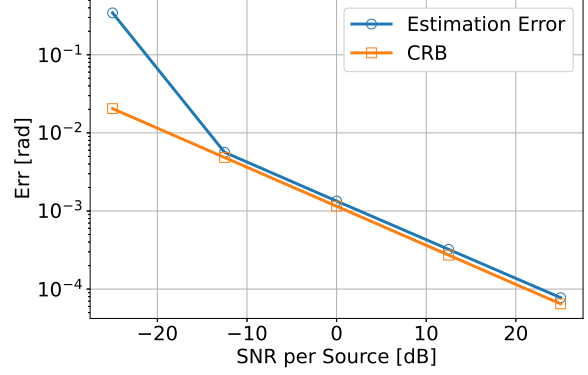


Fig. 5: Performance of the proposed algorithm on two-dimensional MMV ANM. The size of the problem is  $32 \times 32 \times 5$ . Each data point is an average of 20 monte carlo trials. In each trial, the ANM problem is solved using the coordinate descent framework up to  $\text{tol} = 10^{-8}$ .

the vanilla atomic set (7), the following weighted atomic set is employed for enhanced the separability of closely spaced frequencies:

$$\left\{ w(f) \mathbf{a}(f) \otimes \mathbf{c} \mid \phi, f \in [0, 2\pi), [\mathbf{a}(f)]_i = e^{1j(i-1)f} \right\} \quad (28)$$

Let  $\mathcal{A}$  be the vanilla set (6) and let  $\mathcal{A}_w$  be the weighted atomic set (28). The proposed algorithmic framework can be applied to ANM problems with  $\mathcal{A}_w$  as well provided that the first and the second order derivatives  $\frac{dw}{df}, \frac{d^2w}{df^2}$  are available. The key to solve weighted ANM problems is the following sub-problem:

$$\begin{aligned} & \text{Minimize}_{f, \mathbf{c} \in \mathbb{C}^M} \|\mathbf{c}\|_2 + \frac{\zeta}{2} \|\mathbf{Y}_r - w(f) \mathbf{a}(f) \otimes \mathbf{c}\|_2^2 \quad (29) \\ & \text{subject to } f \in [0, 2\pi); \end{aligned}$$

(29) can be solved using Newton’s method similar to the one in algorithm 2. Relevant details is in the appendix [ref]. To demonstrate that the proposed algorithm can be applied to weighted ANM problems, a numerical experiment based on [25] is presented. The problem is to estimate the ground truth frequencies given a noisy MMV observation:

$$\mathbf{Y} = \sum_{i=1}^L P \mathbf{a}(f_i) \otimes \mathbf{c}_i + \mathbf{N} \quad (30)$$

Specifically,  $N = 32$  and  $M = 5$ . In every monte carlo trial each entry of  $\mathbf{N} \in \mathbb{C}^{N \times M}$  is i.i.d. standard complex Gaussian random variable. In all trials,  $L = 5$  is fixed with  $[f_1, f_2, \dots, f_5] = 2\pi [0.1, 0.108, 0.125, 0.2, 0.5]$ . To simplify SNR calculation, for each source  $\|\mathbf{c}_i\|_2 = 1$ . The SNR per source is then defined as  $\text{SNR} = 20 \log_{10}(\frac{P}{\sqrt{M}})$ . Clearly,  $f_1, f_2, f_3$  are three closely spaced frequencies that are hard to differentiate with the  $N = 32$  measurement vectors. Based on [25], the reweighted procedure is used to estimate  $f_i$ :

- Starting with  $k = 0, \varepsilon_0 = 1, \mathbf{R}_0 = N\mathbf{I}$ .
- In the  $k$ -th iteration, the ANM problem with

$$w_k(f) = (\mathbf{a}(f)^H \mathbf{R}_k^{-1} \mathbf{a}(f))^{-1/2} \quad (31)$$

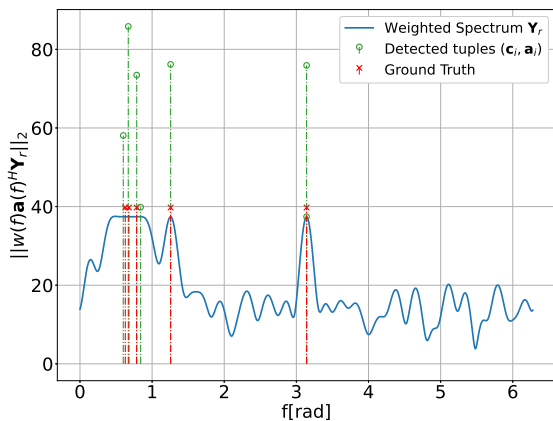


is solved. After obtaining the set  $\mathcal{S}_k$  of tuples  $(\hat{f}_i, \hat{c}_i)$ , the matrix  $\mathbf{R}_{k+1}$  in weighting function is updated:

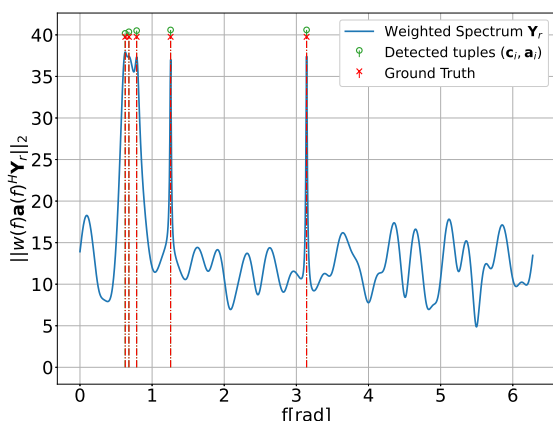
$$\mathbf{R}_{k+1} = \varepsilon_k^{-1} \sum_{i=1}^{|\mathcal{S}_k|} \|\mathbf{c}_i\|_2 \mathbf{a}(\hat{f}_i) \mathbf{a}(\hat{f}_i)^H + N\mathbf{I} \quad (32)$$

$$\varepsilon_{k+1} = \varepsilon_k/2 \quad (33)$$

In all iterations, the value of  $\zeta$  remains the same  $\zeta = (\frac{\ln M}{M})^{1/2} [N \log N + N \log(4\pi \log N)]^{-1/2}$ . As suggested by the formula above, the 0-th iteration  $k = 0$  is the same as solving an unweighted ANM problem. From there, the weighting function is updated such that certain elements in  $\mathcal{A}$  can be better differentiated from others. The iterative process is terminated once  $\varepsilon \leq 0.001$ . The result of this reweighted process is demonstrated in the figure 6. Although the vanilla ANM fails to differentiate the closely spaced frequencies  $f_1, f_2, f_3$ , the three frequencies are identified after one iteration.



(a) 0-th Iteration



(b) 1-st Iteration

Fig. 6: Visualization of the iterative reweighted ANM process at 25 dB SNR. Due to the separation requirement, the outcome of a normal ANM (0-th iteration) is not accurate. With the weighting function based on Capon's beamforming (31), the closely spaced sources can be successfully differentiated given high enough SNR.

The overall performance of the weighted ANM approach for line spectral estimation is provided in figure 7. Each data point is an average of 20 Monte Carlo trials. Each trial includes 4 reweighted ANM problems. In each problem, the coordinate descent algorithm is terminated when the tolerance  $\text{tol} = 10^{-6}$  is satisfied or the maximum 20000 iterations are met. The vanilla ANM problem hits the error floor quickly. With the reweighted technique, the accuracy of the estimation increases with SNR. The CRB value is calculated using the same technique as in the previous section.

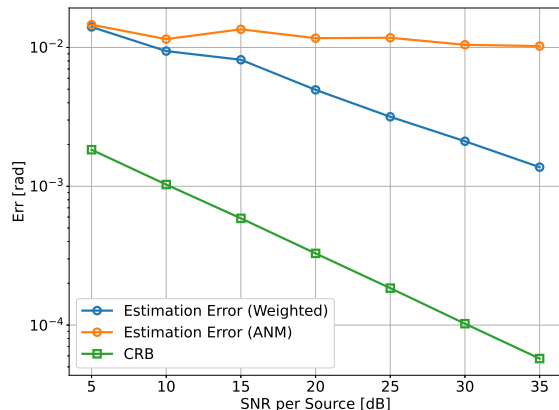


Fig. 7: Iterative Reweighted ANM problems.

The experiment showed that the coordinate descent framework can handle weighted ANM problems. However, it is worth noting the fast computation based on FFT is not available for the weighted atomic set. This is due to the weighting function  $w(f)$ . The complexity of each iteration in algorithm 1 is dominated by evaluating  $w(f)$  over a large number of points. For the weighting function (31), each point takes  $N$  operations to evaluate. Therefore for weighted ANM problems, the proposed method might lose its advantage on algorithmic complexity. Consequently, the strength of the proposed coordinate descent framework in this case is mainly on its flexibility, as it is not trivial to integrate the weighting function  $w(f)$  into a SDP. Yet the proposed method can solve the ANM for a wider range of weighting functions.

#### D. Application to Deconvolution

Using the power of super-resolution method to characterize a linear system has been studied in [12]. In this section, another numerical experiment based on a similar idea is presented for a channel estimation problem in an orthogonal frequency division multiplexing (OFDM) system. Essentially, the objective is to estimate the continuous impulse response of a linear system given its discrete input  $\mathbf{x}$  and output vectors  $\mathbf{y}$ . Let  $x(t)$  and  $y(t)$  be the band-limited continuous-time signals from which  $\mathbf{x}$  and  $\mathbf{y}$  are sampled. Let  $\Delta T$  be the sampling

interval. The signal model in the problem is:

$$\mathbf{y} = \sum_{l=1}^L \mathbf{x}_l c_l + \mathbf{n} \quad (34)$$

$$[\mathbf{y}]_i = y(i\Delta T), \quad [\mathbf{x}_l]_i = x(i\Delta T - \tau_l) \quad (35)$$

Given the sampled discrete signal  $\mathbf{y}$ ,  $\mathbf{x} \in \mathbb{C}^N$ , the objective is to estimate the channel impulse response

$$h(t) = \sum_{l=1}^L c_l \delta(t - \tau_l) \quad (36)$$

and to use the estimated channel to perform equalization such that the subsequent OFDM payloads can be decoded. To model the estimation as ANM problems, taking DFT on both sides of (34) yields:

$$\begin{bmatrix} Y(e^{j\omega_0}) \\ Y(e^{j\omega_1}) \\ \vdots \\ Y(e^{j\omega_{N-1}}) \end{bmatrix} = \sum_{l=1}^L c_l \begin{bmatrix} X(e^{j\omega_0})e^{j\omega_0\tau_l/\Delta T} \\ X(e^{j\omega_1})e^{j\omega_1\tau_l/\Delta T} \\ \vdots \\ X(e^{j\omega_{N-1}})e^{j\omega_{N-1}\tau_l/\Delta T} \end{bmatrix} \quad (37)$$

$$+ \begin{bmatrix} N(e^{j\omega_0}) \\ N(e^{j\omega_1}) \\ \vdots \\ N(e^{j\omega_{N-1}}) \end{bmatrix}$$

where  $Y(e^{j\omega})$ ,  $X(e^{j\omega})$ ,  $N(e^{j\omega})$  denote the DFT of their corresponding vectors. It's straight forward to see that (37) includes an embedded ANM problem on the vector  $Y(e^{j\omega})/X(e^{j\omega})$ . Notice that based on definition of DFT,  $\omega_i = \frac{i}{N}2\pi$ ,  $i = 0, 1, \dots, N-1$ . Therefore the tuple of interest in (37) can be directly modelled as  $(c_l, \mathbf{a}(\frac{\tau_l}{N\Delta T}))$ . From the result of ANM, the analytical channel impulse response can be readily reconstructed and used for equalization.

In this numerical experiment, an OFDM system of 256 subcarriers are considered. Two OFDM symbols are treated as preamble to perform channel estimation. The problem is formulated as a MMV ANM with  $N = 256$ ,  $M = 2$ . In each Monte Carlo trial,  $L = 2$  paths are simulated. Each OFDM symbol includes a cyclic prefix with length  $N/4$ . Correspondingly, the randomly generated path delay is controlled such that  $0 \leq \tau_l < N\Delta T/4$ . Each entry of  $\mathbf{n}$  is sampled from the standard complex normal distribution  $\mathcal{CN}(0, 1)$ . The SNR in the experiment is defined as  $\text{SNR} = 20 \log_{10} \left( \frac{\|\mathbf{x}\|_2 \sqrt{\sum_l |c_l|^2}}{N} \right)$ .

For an illustration purpose, the following figure 8 provides an illustration of the frequency response of the estimated channel at SNR = 10 dB. For comparison, result from the conventional correlation based channel estimation is provided. As indicated by the figure, because of the sparsity, the frequency response of the estimated channel using ANM technique is less noisy than that obtained from correlation. From the perspective of the bit error rate, the ANM-based channel estimation technique yields about 2dB gain across multiple SNR as indicated in figure 9.

## V. DISCUSSIONS AND FUTURE WORKS

The major shortcoming of the proposed method is its sensitivity to the sparsity of the problem. For a typical ANM,

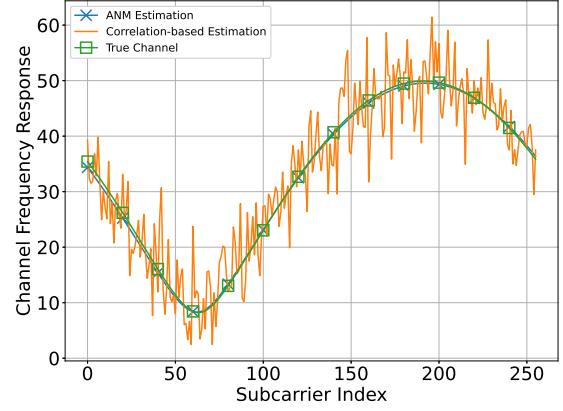


Fig. 8: Estimation results for the frequency response of a 2-path channel at 10dB SNR. Both the true channel frequency response and the ANM based estimation are computed analytically from the path gains and delays. The ANM problem is solved to  $\text{tol} = 10^{-6}$  tolerance.

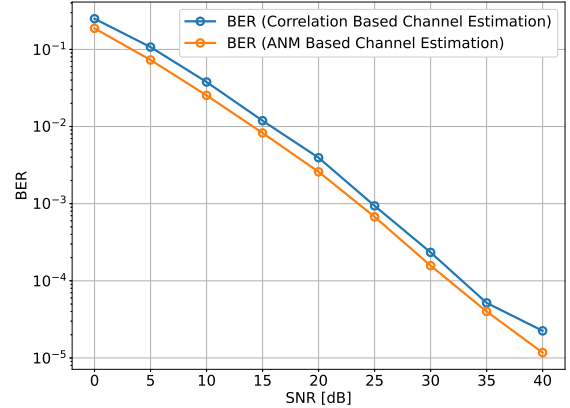


Fig. 9: The bit-error-rate after channel equalization. Each subcarrier carries a randomly selected 4 quadrature-amplitude-modulation symbol (2bits). For every channel realization, the payloads include 10 OFDM symbols.

the sparsity of the problem is reflected in the number of detected line spectra  $L_{\min}$  and the size of the problem  $N$ . In most numerical experiments presented in the previous section, the sparsity of the underlying problem is assumed, i.e.,  $L_{\min} \ll N$ . Suppose in the output of algorithm 1, there are  $|\mathcal{S}|$  tuples detected. Then, algorithm 1 needs at least  $\mathcal{O}(|\mathcal{S}|^2)$  iterations to converge. Consequently, for a  $L$ -sparse ANM problem with the simplest atomic set (6), the proposed coordinate descent method yields computational complexity  $\mathcal{O}(L^2 N \log N)$ . Thus, for non-sparse ANM problem the coordinate descent method becomes highly inefficient. A typical example is the trials in section IV-A with  $\zeta = 1/\sqrt{N}$  instead of  $\zeta = 1/\sqrt{N \log N/4}$ . The choice  $\zeta = 1/\sqrt{N}$  yields  $L_{\min} \sim \mathcal{O}(N^2)$ , which makes the overall complexity for the proposed method  $\mathcal{O}(N^3 \log N)$ . In such cases, conventional

interior-point solvers or ADMM for the SDP formulation of ANM are still preferred as they are not sensitive to the sparsity of the problem.

Part of the advantage of the coordinate descent method is its flexibility. In practice, there are many atomic sets with which the corresponding ANM problems cannot be easily formulated as SDP. In such cases, the conventional deciplined interior-point solvers are not available. However, these problem can still be solved by the proposed coordinate descent framework as long as sub-problems (18) are solvable. Under such assumptions, more ANM problems become tracable. A recently developed example is [26] where the authors employed a carefully developed atomic set for sparse phase retrieval and principle component analysis. In [26], a generic method similar to the proposed coordinate descent framework was used simply because that the SDP formulation is intractable. Although the sub-problem analogous to (18) was also too difficult to solve such that the authors only solved it approximately, the performance of their generic method was still better than most presented baselines for sparse phase retrieval.

There are plenty of open research questions along the track of using coordinate descent method to solve ANM problems. From the perspective of applications, many previously untracable atomic sets can now be considered. For instance, the atomic set of interest can be a continuous manifold produced by a pretrained neural network for a speific image processing task. From the perspective of optimization, the proposed coordinate descent framwork can be accelerated with better initialization. The method itself can also be further optimized to get rid of the ambiguity mentioned in remark 3 or to work with a lower oversampling ratio  $r = 8$  with the help of a modified algorithm 2 that uses a line-search strategy.

## VI. CONCLUSION

In this paper, an efficient method for sparse atomic norm minimization is proposed. The method is based on the classic idea of coordinate descent. It bypasses the SDP formulation of ANM in conventional convex optimization and converges to the global optimal point by solving non-convex sub-problems. The method is essentially matrix-free and low-complexity and thus offers a scalable solution for large-scale ANM problems. Several numerical experiments are presented to confirm the flexibility and efficiency of the coordinate descent method. To conclude, the proposed method can be a potential candidate for a wide range of applications of atomic norm minimization.

## REFERENCES

- [1] Yuejie Chi, Louis L Scharf, Ali Pezeshki, and A Robert Calderbank, "Sensitivity to basis mismatch in compressed sensing," *IEEE Transactions on Signal Processing*, vol. 59, no. 5, pp. 2182–2195, 2011.
- [2] Emmanuel J Candès and Carlos Fernandez-Granda, "Towards a mathematical theory of super-resolution," *Communications on pure and applied Mathematics*, vol. 67, no. 6, pp. 906–956, 2014.
- [3] Yuejie Chi and Maxime Ferreira Da Costa, "Harnessing sparsity over the continuum: Atomic norm minimization for superresolution," *IEEE Signal Processing Magazine*, vol. 37, no. 2, pp. 39–57, 2020.
- [4] Lieven Vandenberghe Martin S Andersen, Joachim Dahl, "Cvxopt: A python package for convex optimization, version 1.1.6," 2013.
- [5] Thomas Lundgaard Hansen and Tobias Lindstrøm Jensen, "A fast interior-point method for atomic norm soft thresholding," *Signal Processing*, vol. 165, pp. 7–19, 2019.

- [6] Yue Wang and Zhi Tian, "Ivdst: A fast algorithm for atomic norm minimization in line spectral estimation," *IEEE Signal Processing Letters*, vol. 25, no. 11, pp. 1715–1719, 2018.
- [7] Zai Yang and Lihua Xie, "Exact joint sparse frequency recovery via optimization methods," *IEEE Transactions on Signal Processing*, vol. 64, no. 19, pp. 5145–5157, 2016.
- [8] Yu Zhang, Yue Wang, Zhi Tian, Geert Leus, and Gong Zhang, "Low-complexity gridless 2d harmonic retrieval via decoupled-anm covariance reconstruction," in *2020 28th European Signal Processing Conference (EUSIPCO)*, 2021, pp. 1876–1880.
- [9] Zai Yang, Lihua Xie, and Petre Stoica, "Vandermonde decomposition of multilevel toeplitz matrices with application to multidimensional super-resolution," *IEEE Transactions on Information Theory*, vol. 62, no. 6, pp. 3685–3701, 2016.
- [10] Zai Yang and Lihua Xie, "Enhancing sparsity and resolution via reweighted atomic norm minimization," *IEEE Transactions on Signal Processing*, vol. 64, no. 4, pp. 995–1006, 2016.
- [11] Badri Narayan Bhaskar, Gongguo Tang, and Benjamin Recht, "Atomic norm denoising with applications to line spectral estimation," *IEEE Transactions on Signal Processing*, vol. 61, no. 23, pp. 5987–5999, 2013.
- [12] Parikshit Shah, Badri Narayan Bhaskar, Gongguo Tang, and Benjamin Recht, "Linear system identification via atomic norm regularization," in *2012 IEEE 51st IEEE Conference on Decision and Control (CDC)*, 2012, pp. 6265–6270.
- [13] Yue Wang, Yu Zhang, Zhi Tian, Geert Leus, and Gong Zhang, "Super-resolution channel estimation for arbitrary arrays in hybrid millimeter-wave massive mimo systems," *IEEE Journal of Selected Topics in Signal Processing*, vol. 13, no. 5, pp. 947–960, 2019.
- [14] Jerome Friedman, Trevor Hastie, and Rob Tibshirani, "Regularization paths for generalized linear models via coordinate descent," *Journal of statistical software*, vol. 33, no. 1, pp. 1, 2010.
- [15] Ryan J Tibshirani, *The solution path of the generalized lasso*, Stanford University, 2011.
- [16] Yuejie Chi, "Joint sparsity recovery for spectral compressed sensing," in *2014 IEEE International Conference on Acoustics, Speech and Signal Processing (ICASSP)*. IEEE, 2014, pp. 3938–3942.
- [17] Babak Mamandipoor, Dinesh Ramasamy, and Upamanyu Madhoo, "Newtonized orthogonal matching pursuit: Frequency estimation over the continuum," *IEEE Transactions on Signal Processing*, vol. 64, no. 19, pp. 5066–5081, 2016.
- [18] Anupama Govinda Raj and James H McClellan, "Single snapshot super-resolution doa estimation for arbitrary array geometries," *IEEE Signal Processing Letters*, vol. 26, no. 1, pp. 119–123, 2018.
- [19] Xingguo Li, Tuo Zhao, Raman Arora, Han Liu, and Mingyi Hong, "On faster convergence of cyclic block coordinate descent-type methods for strongly convex minimization," *The Journal of Machine Learning Research*, vol. 18, no. 1, pp. 6741–6764, 2017.
- [20] Amir Beck and Luba Tretuashvili, "On the convergence of block coordinate descent type methods," *SIAM J. Optim.*, vol. 23, pp. 2037–2060, 2013.
- [21] T. L. Hansen and T. L. Jensen (2018), "fast-ast," [Online]. Available: <https://github.com/thomaslundgaard/fast-ast>.
- [22] The MathWorks Inc., "Matlab version: 9.13.0 (r2022b)," 2022.
- [23] Zhi Tian, Zhe Zhang, and Yue Wang, "Low-complexity optimization for two-dimensional direction-of-arrival estimation via decoupled atomic norm minimization," in *2017 IEEE International Conference on Acoustics, Speech and Signal Processing (ICASSP)*, 2017, pp. 3071–3075.
- [24] Zai Yang, Yi-Lin Mo, Gongguo Tang, and Zongben Xu, "Separation-free spectral super-resolution via convex optimization," *arXiv preprint arXiv:2211.15361*, 2022.
- [25] Zai Yang and Lihua Xie, "Enhancing sparsity and resolution via reweighted atomic norm minimization," *IEEE Transactions on Signal Processing*, vol. 64, no. 4, pp. 995–1006, 2016.
- [26] Andrew D. McRae, Justin Romberg, and Mark A. Davenport, "Optimal convex lifted sparse phase retrieval and pca with an atomic matrix norm regularizer," *IEEE Transactions on Information Theory*, vol. 69, no. 3, pp. 1866–1882, 2023.

## APPENDIX A

### SOLVING TWO-DIMENSIONAL MMV ANM

The key to solve two-dimensional MMV ANM problem is the sub-problem of a single element (24) which is simplified

as:

$$\underset{\mathbf{c}_i \in \mathbb{C}^M, f_i^1, f_i^2}{\text{Minimize}} \quad \|\mathbf{c}_i\|_2 - \zeta \langle \mathbf{Y}_r, \mathbf{a}(f_i^1) \otimes \mathbf{a}(f_i^2) \otimes \mathbf{c}_i \rangle + \frac{\zeta N^2 \|\mathbf{c}_i\|_2^2}{2} \quad (38)$$

The inner-product in the vector space of three-dimensional tensor is defined as

$$\langle \mathbf{X}, \mathbf{Y} \rangle = \sum_{i,j,k} \text{Re} \left\{ [\mathbf{X}]_{i,j,k}^* [\mathbf{Y}]_{i,j,k} \right\} \quad (39)$$

Let  $\hat{\mathbf{c}} = \mathbf{c} / \|\mathbf{c}\|_2$ . As in (20)-(22), (38) also admits a separable solution:

$$(f_1^*, f_2^*) = \underset{f_1, f_2}{\text{argmax}} \|\mathbf{Y}_r \odot (\mathbf{a}(f_1) \otimes \mathbf{a}(f_2) \otimes \mathbf{1})\|_2 \quad (40)$$

$$\hat{\mathbf{c}}^* = \underset{\hat{\mathbf{c}}, \|\hat{\mathbf{c}}\|_2=1}{\text{argmax}} \|\mathbf{Y}_r \odot (\mathbf{a}(f_1^*) \otimes \mathbf{a}(f_2^*) \otimes \hat{\mathbf{c}})\|_2 \quad (41)$$

The role of  $\|\mathbf{c}\|_2$  is the same as that of  $c$  in (21). The optimal  $\|\mathbf{c}\|_2^*$  involves a shrink and thresholding step. Let  $\eta = \|\mathbf{Y}_r \odot (\mathbf{a}(f_1^*) \otimes \mathbf{a}(f_2^*) \otimes \hat{\mathbf{c}}^*)\|_2$ . Then,

$$\|\mathbf{c}\|_2^* = \begin{cases} 0, & \eta \leq \frac{1}{\zeta} \\ \frac{1}{N^2} \left( \eta - \frac{1}{\zeta} \right), & \eta > \frac{1}{\zeta} \end{cases} \quad (42)$$

The key step is still (40). Similar to algorithm 2, the following procedure is employed to solve (40):

- To start with, an oversampled two-dimensional FFT is performed on the first two dimensions of  $\mathbf{Y}_r$  to evaluate  $\|\mathbf{Y}_r \odot (\mathbf{a}(f_1) \otimes \mathbf{a}(f_2) \otimes \mathbf{1})\|_2$  on a fine mesh of grid points  $(f_1, f_2)$ . The coordinate of the maximum over the mesh is used as the starting point.
- Starting with the maximum  $(f_1, f_2)$  over the mesh, use Newton's method to solve for the off-grid maximum until convergence.

The methodology is the same, as long as the initial mesh is dense enough, the Newton's method can converge to the global maximum  $(f_1^*, f_2^*)$  of the non-convex function  $\|\mathbf{Y}_r \odot (\mathbf{a}(f_1) \otimes \mathbf{a}(f_2) \otimes \mathbf{1})\|_2$ . Plugging in  $(f_1^*, f_2^*)$  to (41), (42) then completes the solution to (24).

## APPENDIX B SOLVING WEIGHTED MMV ANM

The key to solve weighted MMV ANM problem is the sub-problem of a single tuple (29), which is then simplified as:

$$\underset{\mathbf{c} \in \mathbb{C}^M, f}{\text{Minimize}} \quad \|\mathbf{c}\|_2 - \zeta \langle \mathbf{Y}_r, w(f) \mathbf{a}(f) \otimes \mathbf{c} \rangle + \frac{\zeta w^2(f) N^2 \|\mathbf{c}\|_2^2}{2} \quad (43)$$

Different from unweighted cases of DFT atomic set, the second order term in (43) also depends on  $f$  because of the weights  $w^2(f)$ . Let  $\hat{\mathbf{c}} = \mathbf{c} / \|\mathbf{c}\|_2$ . The objective function in (43) can be further re-organized as:

$$\begin{aligned} & \|\mathbf{c}\|_2 - \zeta \langle \mathbf{Y}_r, w(f) \mathbf{a}(f) \otimes \mathbf{c} \rangle + \frac{\zeta w^2(f) N^2 \|\mathbf{c}\|_2^2}{2} \quad (44) \\ & = w(f) \zeta \|\mathbf{c}\|_2 \left( \frac{1}{\zeta w(f)} - \langle \mathbf{Y}_r, \mathbf{a}(f) \otimes \hat{\mathbf{c}} \rangle \right) + \frac{\zeta w^2(f) N^2 \|\mathbf{c}\|_2^2}{2} \end{aligned}$$

(43) indicates a separable solution for (29) as following:

$$f^* = \underset{f}{\text{argmax}} \|\mathbf{Y}_r^H \mathbf{a}(f)\|_2 - \frac{1}{\zeta w(f)} \quad (45)$$

$$\hat{\mathbf{c}}^* = \underset{\hat{\mathbf{c}}, \|\hat{\mathbf{c}}\|_2=1}{\text{argmax}} \langle \mathbf{Y}_r, \mathbf{a}(f^*) \otimes \hat{\mathbf{c}} \rangle \quad (46)$$

The shrinkage and thresholding step on  $\|\mathbf{c}\|_2$  becomes slightly different as it involves the weighting function  $w(f)$ . Let  $\eta = \langle \mathbf{Y}_r, \mathbf{a}(f^*) \otimes \hat{\mathbf{c}}^* \rangle$ . The optimal  $\|\mathbf{c}\|_2^*$  is calculated from the following:

$$\|\mathbf{c}\|_2^* = \begin{cases} 0, & \eta \leq \frac{1}{w(f)\zeta} \\ \frac{1}{w(f)N^2} \left( \eta - \frac{1}{w(f)\zeta} \right), & \eta > \frac{1}{w(f)\zeta} \end{cases} \quad (47)$$

(47) clearly indicates the functionality of  $w(f)$  which has an impact on the threshold  $1/\zeta$ . Unfortunately,  $w(f)$  also makes it harder to solve the key step (45) as FFT along is not enough to evaluate  $\|\mathbf{Y}_r^H \mathbf{a}(f)\|_2 - \frac{1}{\zeta w(f)}$  on a large number of points. However, the methodology remains the same:

- To start with, an oversampled two-dimensional FFT is performed on the first dimension of  $\mathbf{Y}_r$  to evaluate  $\|\mathbf{Y}_r^H \mathbf{a}(f)\|_2$  on a fine grid points over  $[0, 2\pi)$ . Additionally,  $\frac{1}{w(f)\zeta}$  is also evaluated over the same fine grid. The coordinate of the maximum  $\|\mathbf{Y}_r^H \mathbf{a}(f)\|_2 - \frac{1}{\zeta w(f)}$  over the grid is used as the starting point.
- Starting with the maximum on-grid  $f$ , use Newton's method to solve for the off-grid maximum until convergence. In each Newton's step, the first and the second order derivatives  $\frac{dw}{df}$ ,  $\frac{d^2w}{df^2}$  need to be computed.

Once the off-grid maximum  $f^*$  is found, plugging  $f^*$  into (47), (46) completes the solution.